Published by
NIGERIAN SOCIETY OF PHYSICAL SCIENCES
Available online @ https://journal.nsps.org.ng/index.php/jnsps

J. Nig. Soc. Phys. Sci. 5 (2023) 1350

Journal of the Nigerian Society of Physical Sciences

Numerical Simulation of Nonlinear and Non-Isothermal Liquid Chromatography for Studying Thermal Variations in Columns Packed with Core-Shell Particles

Abdulaziz G. Ahmad[a,b,*], Nnamdi F. Okechi[a], David U. Uche[a,c], Abdulwasiu O. Salaudeen[d]

[a]*Department of Mathematics Programme, National Mathematical Centre Abuja, Nigeria*
[b]*Department of Applied Mathematics, Federal University of Technology Babura, Nigeria*
[c]*Department of Mathematics, University of Abuja, Nigeria*
[d]*Department of Applied Mathematics (Chemistry Unit) Programme, National Mathematical Centre Abuja, Nigeria*

Abstract

A high-resolution flux-limiting semi-discrete finite volume scheme (HR-FVS) is applied in this study to numerically approximate the nonlinear and non-isothermal flow of one-dimensional lumped kinetic model (1D-LKM), for a fixed-bed column loaded with core-shell particles. The developed model comprise a system of convection-dominated partial differential for mass and energy balances in the mobile phases coupled with differential equation and algebraic equation in the stationary phase. The solution of the model equations is obtained by utilizing a HR-FVS, the scheme has second-order accuracy even on the grid coarse and its explicit nature has the potential to resolve the arisen sharp discontinuities in the solution profiles. A second-order total variation diminishing (TVD) Runge-Kutta technique is used to solve the system of ODEs in time. Several forms of a single-solute mixture are produced to investigate the influences of the fractions of core radius on thermal waves and concentration fronts. Moreover, a particular criterion is introduced for analyzing the performance of the underlying process and to identify the optimal parameter values of the fraction of core radius.

DOI:10.46481/jnsps.2023.1350

Keywords: Non-isothermal chromatography, Non-linear isotherm, One-dimensional lumped kinetic model, High-resolution scheme

Article History :
Received: 15 January 2023
Received in revised form: 06 March 2023
Accepted for publication: 10 March 2023
Published: 24 April 2023

Communicated by: J. Ndam

1. Introduction

In recent years, chemical engineers and researchers are increasingly interested in High-performance liquid chromatography (HPLC) to further improve the performance of classical column. An innovative and valuable tool used for the separation and quantification of the multi-component mixture due to the different affinities of adsorption for the components is known as HPLC. This technique is commonly used in the chemical, pharmaceutical and food industries where the traditional operations in the thermal unit, such as distillation and extraction, are unsuitable [1–3]. For both large and preparative scales this process is equally popular, especially for the purification of proteins and other higher valuable products. Figure 1 illustrates a typical demonstration of a single-column HPLC. Here, the sample is injected via inner region, which propagates the

*Corresponding author tel. no: +234 80326117615
Email address: agarbaahmad@yahoo.com (Abdulaziz G. Ahmad)

solute along z-direction of the column by advection and axial-dispersion.

Separation efficiency of HPLC can be made better by using small diameter particles to be loaded into the column in order to reduced the resistance of intra-particulate mass transfer due to short diffusion distances [4–6]. These loaded core-shell particles were designed and operated in the columns of HPLC to contempt the utilization of technical types of equipment. Recently, the use of core-shell particles has created significant interest in both analytical and preparative liquid chromatography. It was applied to segregate peptides and other molecules, such as nucleotides, and proteins [5, 7]. Aside from that, several theoretical investigations involving the use of core-shell particles were made by analyzing models of liquid chromatography in one-dimensional (1D) forms [1, 3]. Kaczmarski and Guichon [8] consider the general rate model to substantiate the benefits of thin-shell coated beads. Also, the same general rate model is employed by Gu et al. [4] to optimize and examine the influences of core radius fraction in isocratic elution of multi-component mixture. Several authors have recently emphasized the importance of studying the differences of core-shell and fully porous particles by formulating and solving a number of chromatographic models via core-shell particles [9–11].

Inspired by the work of Brandt, et al., [12]. Temperature has a wide impact on all chromatography processes, and there are several ways to analyze its significance [13, 14]. For example, increasing the temperature decreases viscosity while rising solubility and diffusivity. Moreover, the peak shape, the efficiency of the column, complete-time analysis and retention time has temperature influences due to the thermodynamics, and adsorption kinetics are temperature-dependent [15, 16]. Further, the use of a steady condition of temperature during the process increases reproducibility. Even though, effects of thermal property are typically ignored in the columns of liquid chromatographic because the effect of heat adsorption is assumed to be inconsiderable, many more chromatographers have figured out that temperature is critical to the process optimization [13]. On contrarily, a number of researchers have investigated thermal impacts in gas chromatography [17–19]. There are additional contributions in the literature that examine the thermal influences in liquid chromatography columns, which are also accessible [3, 13, 14, 20–24].

A number of mathematical models for simulating the underlying chemical process at various extent of complexities are available in the literature to aid in the understanding of physical phenomena [15, 16, 25, 26]. This modeling approach allows us to comprehend what occurs within the column, and also during the separation process. The most influential and widely employed models that exist in the literature include the equilibrium dispersive model (EDM), the model based on linearized driving force, the lumped kinetic model (LKM), and the general rate model (GRM) [1–3, 27]. The mass transfer rate in the EDM is considered to be infinite, but the local concentration's rate of change in the LKM is presumed to be finite [1–3]. GRM is a model that incorporates intra-particle diffusion which includes mass transfer across the interface among the both phases (i.e., stationary and mobile). It is also referred to as the most comprehensive model [1].

A nonlinear 1D-LKM incorporating core-shell particles is numerically approximated in this article. This work extends the analysis of 1D-LKM non-isothermal model [28]. Unlike the past study, this prevailing non-isothermal 1D-LKM helps to examine the effect of core radius fractions on thermal and concentration fronts along the axial gradients of the eluent in the column. The formulated model comprises of a system of convection-dominated partial differential for mass and energy balances in the mobile phases coupled with differential and algebraic equations in the stationary phase. The solution of the model is obtained by utilizing a HR-FVS. The scheme deals with integral form of conservation laws and also it has potential to produce numerical result that can resolve sharp discontinuity and achieve higher order accuracy. Afterwards, a Runge-Kutta approach for second-order TVD is used to simulate the system of ODEs in term of time [30]. Some certain test problems are considered to illustrate the simultaneous elution of thermal and concentration fronts. Furthermore, we hope that the key parameters that influence the elution profiles within the column are identified.

The article arranged as follows. In Section 2, a nonlinear and non-isothermal 1D-LKM incorporated with core-shell particles is developed. In Section 3, the numerical simulation of the non-isothermal 1D-LKM is obtained for the boundary conditions discussed by Dankwerts condition. Section 4 outlines a number of simulated case problems, and ultimately, Section 5 contains the conclusions.

2. Mathematical model formulation of the process

In this section, the following assumptions are employed to configure and develop the model equations: (i) the column is considered to be thermally insulated and homogeneously loaded with ore-shell particles, (ii) the fluid is incompressible with constant rate of volumetric flow, (iii) the stationary and mobile phases have negligible interaction between them, (iv) the axial heat conductivity coefficient are independent of the flow rate, (v) the temperature does not affect physical properties such as density, viscosity, heat capacity, or coefficients of transport (e.g. axial dispersion and heat conductivity), (vi) the linear driving force model is utilized to determine the overall adsorption rate, and (vii) the heat transfer resistance of the solid phase is concentrated at the particle surface.

Let t symbolize the coordinate time while the coordinate in axial direction alongside the column length is donated as z, the symbol R_p represents the unvarying size of cored beads parked in the column and fraction of core radius is $\eta_{core} = R_c/R_p$ where R_c symbolized the radius of the inert core. The solute will propagate via the column's z-direction with advection and axial-dispersion. The one-dimensional equations for the balance of mass and the heat for a solute mixture elution in the mobile phase via column loaded with spherical core beads are

expressed as

$$\frac{\partial c}{\partial t} + u\frac{\partial c}{\partial z} - D_z\frac{\partial^2 c}{\partial z^2} + F(1-\eta_{core})k(\phi^* - \phi) = 0, \quad (1)$$

$$\frac{\partial T}{\partial t} + u\frac{\partial T}{\partial z} - \frac{\lambda_z}{\xi_f}\frac{\partial^2 T}{\partial z^2} + F(1-\eta_{core})\frac{3h_p}{R_p\xi_f}(T - T_s) = 0. \quad (2)$$

From the equations above, the symbol c represents the solute mixture in the mobile phase, the interstitial velocity is donated as u, the symbol D_z represents the axial-dispersion coefficient, while the symbol ϵ denotes the external porosity and the phase ratio is expressed as $F = \frac{1-\epsilon}{\epsilon}$. Also, the symbol ϕ represents the non-equilibrium average loading of concentration in the particular solid phase, in the mobile phase the temperature is indicated as T, and coefficients of heat conductivity along with the axial coordinates is represented as λ_z. Moreover, $\xi_e = \rho^s c_p^s$, $\xi_f = \rho^l c_p^l$, ρ^s and ρ^l indicate the solid and liquid phases' densities per unit volume, respectively, T_s stands for the temperature of the stationary phase, while c_p^s and c_p^l symbolize the solid and liquid phases' respective heat capacities.

In the solid phase, the corresponding mass and heat balance equations are written as

$$\frac{\partial \phi}{\partial t} = k(\phi^* - \phi), \quad (3)$$

$$\frac{\partial T_s}{\partial t} = \frac{-\Delta H_A}{\xi_e}\frac{\partial \phi}{\partial t} + \frac{3h_p}{R_p\xi_e}(T - T_s). \quad (4)$$

From the equations above, the symbol k stands for the mass transfer rate coefficient, ΔH_A represents the enthalpy of adsorption and the coefficient for heat transfer among the mobile and solid phases is symbolized as h_p. For the ι-th number of components in the mixture, the symbol $\phi^*(c, T_s)$ shows a temperature dependency relationship among the specific phase in solid part of concentration at equilibrium ϕ and the temperature, is defined as [16]

$$\phi^*(c, T_s) = \frac{a_{\text{ref}} c \exp^{\left[\frac{-\Delta H_A}{R_g}\left(\frac{1}{T_s} - \frac{1}{T_{\text{ref}}}\right)\right]}}{1 + b_\iota^{\text{ref}} c_\iota \exp^{\left[\frac{-\Delta H_A}{R_g}\left(\frac{1}{T_s} - \frac{1}{T_{\text{ref}}}\right)\right]}}, \quad \iota = 1, \cdots, N_c. \quad (5)$$

Here, the coefficient a_{ref} is symbolizing the Henry's constant at a reference temperature, the symbol b_ι^{ref} is representing the nonlinearity coefficients, the symbol T_{ref} represents the reference temperature, and R_g is universal gas constant. In addition, the model includes the following additional dimensionless parameters, which minimize the parameters in terms of number, this facilitates the analysis of the model.

$$\text{Pe}_{z,M} = \frac{Lu}{D_z}, \quad \text{Pe}_{z,H} = \frac{\xi_f L u}{\lambda_z}, \quad x = \frac{z}{L}, \quad \tau = \frac{ut}{L},$$
$$\kappa = \frac{Lk}{u}, \quad \beta_s = \frac{3Lh_p}{uR_p\xi_e}, \quad \beta_L = \frac{3Lh_p}{uR_p\xi_f}, \quad (6)$$

The column length is represented by the symbol L, and the Peclet-numbers of both heat and the mass transfer via axial direction are indicated by the symbols $\text{Pe}_{z,H}$ and $\text{Pe}_{z,M}$, accordingly. On utilizing Eq. (6) in Eqs. (1)-(4), we get the following equations below after some manipulations

$$\frac{\partial c}{\partial \tau} = -\frac{\partial c}{\partial x} + \frac{1}{\text{Pe}_{z,M}}\frac{\partial^2 c}{\partial x^2} - F(1-\eta_{core})\kappa(\phi^* - \phi), \quad (7)$$

$$\frac{\partial T}{\partial \tau} = -\frac{\partial T}{\partial x} + \frac{1}{\text{Pe}_{z,H}}\frac{\partial^2 T}{\partial x^2} - F(1-\eta_{core})\beta_L(T - T_s), \quad (8)$$

$$\frac{\partial \phi}{\partial \tau} = \kappa(\phi^* - \phi), \quad (9)$$

$$\frac{\partial T_s}{\partial \tau} = \frac{-\Delta H_A}{\xi_e}\frac{\partial \phi}{\partial \tau} + \beta_s(T - T_s). \quad (10)$$

Appropriate initial conditions that are suitable for the computational solution of the model equations (c.f. Eqs. (7)-(10)) in the range $0 \le x \le 1$. The following are the initial conditions for an equilibrated column:

$$c(x, \tau = 0) = c_{\text{init}}, \quad T(x, \tau = 0) = T_{\text{init}},$$
$$\phi(x, \tau = 0) = \phi^*_{\text{init}}, \quad T_s(x, \tau = 0) = T_{\text{init}}. \quad (11)$$

Here, the initial temperature is represented by T_{init}, the symbol c_{init} is the initial equilibrated concentration of the single component solute, and ϕ^*_{init} is obtained from Eq. (5). The inflow conditions which Dankwert's boundary conditions (BCs) investigate at the column inlet are listed below [9, 31].

The injections in the inner circular region are described as follows:

$$c(x=0,\tau) - \frac{1}{\text{Pe}_{z,M}}\frac{\partial c_i(x=0,\tau)}{\partial x} = \begin{cases} c_{\text{inj}}, & \text{if } 0 \le \tau \le \tau_{\text{inj}}, \\ 0, & \text{if } \tau > \tau_{\text{inj}}, \end{cases} \quad (12a)$$

$$T(x=0,\tau) - \frac{1}{\text{Pe}_{z,H}}\frac{\partial T(x=0,\tau)}{\partial x} = \begin{cases} T_{\text{inj}}, & \text{if } 0 \le \tau \le \tau_{\text{inj}}, \\ T_{\text{ref}}, & \text{if } \tau > \tau_{\text{inj}}. \end{cases} \quad (12b)$$

In this Eq. (12a), c_{inj} represents the concentration of the injected component, the dimensionless time of injection is represented by τ_{inj}, and T_{inj} represents the temperature of the injected component. Moreover, the thermal conditions at the boundary provided by Eq. (12b) allow the temperature of the injection sample to fluctuate. Further, the injected temperature donated by T_{inj} could be adjusted from the reference temperature of the bulk phase T_{ref}.

At the right end of the column, the Neuman conditions are considered:

$$\frac{\partial c(x=1,\tau)}{\partial x} = 0, \quad \frac{\partial T(x=1,\tau)}{\partial x} = 0. \quad (12c)$$

The chromatographic process mathematical model is now complete. The subsequent task is to employ the suggested flux-limiting HR-FVS in order to solve the developed model equations.

3. Numerical scheme

In order to approximate the current model equations numerically, a flux-limiting semi-discrete method HR-FVS is applied,

Table 1: Values of the model parameters used in the test problems

Parameters	Values
Column length	$L = 4.0\,cm$
Radius of the column	$R = 0.2\,cm$
Radius of solid particle	$R_p = 0.004\,cm$
Interstitial velocity	$u = 1.5\,cm/min$
Porosity	$\epsilon = 0.4$
Density of heat capacity of solid	$\xi_f = 4\,kJ/l$
Density of heat capacity of liquid	$\xi_e = 4\,kJ/l$
Axial dispersion coefficient	$D_z = 0.01\,cm^2/min$
Axial conductivity coefficient	$\lambda_z = 0.04\,kJcm^{-1}min^{-1}$
Mass transfer coefficient	$k = 1\,cm/min$
Heat transfer coefficient	$h_p = 1\,W(cm^2K)^{-1}$
Reference temperature	$T_{ref} = 300\,K$
Initial temperature	$T_{init} = T_{ref}$
Inlet temperature	$T_{inj} = T_{ref}$
Initial concentration	$c_{init} = 0\,mol/l$
Inlet concentration	$c_{inj} = 1\,mol/l$
Dimensionless injection time	$\tau_{inj} = 1.5$
Adsorption equilibrium constant	$a_{ref} = 1$

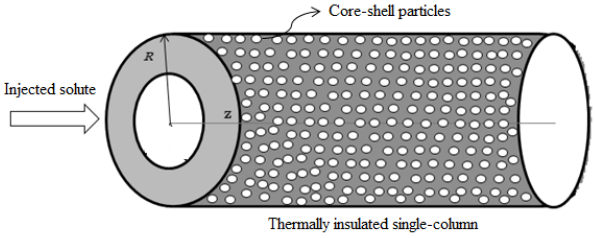

Figure 1: Sketch of solute injection in the thermally insulated chromatographic column incorporating core-shell particles

which have been widely discussed in the literature for approximating 1D-models [9, 10]. To simulate the ODE system in term of time, the second-order TVD Runge-Kutta method is used.

For the derivation of this numerical scheme, let us descritise the computational domain. Let N stand for the number descritisation, $x_{l+\frac{1}{2}}$ to be the interval of left and right boundaries, Δx is the cell width and x_l symbolizes the cell center. Further, let us assign the following

$$x_{N+\frac{1}{2}} = L, \quad x_{\frac{1}{2}} = 0, \quad x_{l+\frac{1}{2}} = l\Delta x_l, \tag{13}$$

$$x_l = \frac{x_{l-\frac{1}{2}} - x_{l+\frac{1}{2}}}{2}, \quad \Delta x_l = x_{l-\frac{1}{2}} - x_{l+\frac{1}{2}} = \frac{L}{N+1}. \tag{14}$$

The domain of cartesian grid $[0, 1]$ that is fully covered by the cells $\Psi_l = x_{l-\frac{1}{2}} - x_{l+\frac{1}{2}}$ for $l \geq 1$. Furthermore, the average initial data $w_l(0)$ in each interval are formulated as

$$w_l(0) = \frac{1}{\Delta x}\int_{x_{l-\frac{1}{2}}}^{x_{l+\frac{1}{2}}} w(x,0)dx, \quad w \in \{c, T, q, q*\}, \quad l = 1, 2, \cdots, N. \tag{15}$$

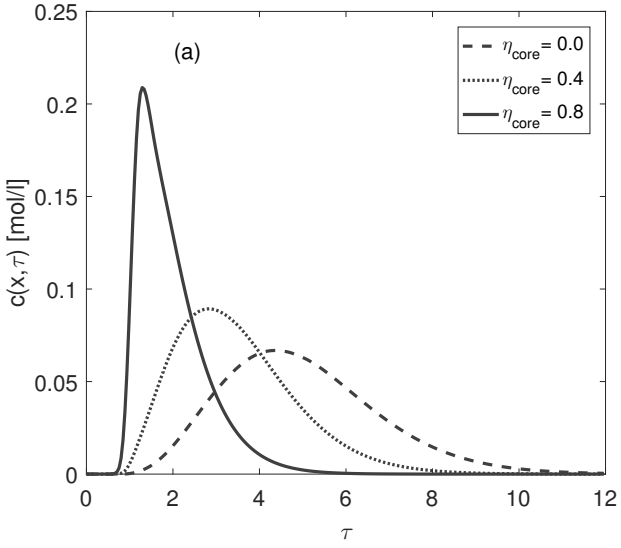

Figure 2: These display the non isothermal single-solute elution profile for distinct values of fraction of core radius η_{core}. Specifically, $\Delta H_A = -10\,kJ/mol$. Table 1 lists all of the other parameter values that were chosen

Once we discretized the computational domain and the associated initial data for $\tau = 0$ is specified for each mesh interval, the subsequent task is to employ the proposed scheme. Integrations of Eqs. (7)-(10) over Ψ_l give

$$\frac{dc_l}{d\tau} = -\frac{\left(c_{l+\frac{1}{2}} - c_{l-\frac{1}{2}}\right)}{\Delta x_l} + \frac{1}{\Delta x_l \mathrm{Pe}_{z,M}}\left[\left(\frac{\partial c}{\partial x}\right)_{l+\frac{1}{2}} - \left(\frac{\partial c}{\partial x}\right)_{l-\frac{1}{2}}\right] \tag{16}$$

$$- F\kappa(\phi_l^* - \phi_l),$$

$$\frac{dT_l}{d\tau} = -\frac{\left(T_{l+\frac{1}{2}} - T_{l-\frac{1}{2}}\right)}{\Delta x_l} + \frac{1}{\Delta x_l \mathrm{Pe}_{z,H}}\left[\left(\frac{\partial T}{\partial x}\right)_{l+\frac{1}{2}} - \left(\frac{\partial T}{\partial x}\right)_{l-\frac{1}{2}}\right] + \tag{17}$$

$$- F\beta_L(T_l - T_{s,l}),$$

$$\frac{d\phi_l}{d\tau} = \kappa(\phi_l^* - \phi_l), \tag{18}$$

$$\frac{dT_{s,l}}{d\tau} = \frac{-\Delta H_A}{\xi_e}\kappa(\phi_{l,j}^* - \phi_{1,l,j}) + \beta_s(T_l - T_{s,l}). \tag{19}$$

The derivatives appearing in Eqs. (16) and (17) are approximated as

$$\left[\frac{\partial c}{\partial x}\right]_{l\pm\frac{1}{2}} = \pm\left[\frac{c_{l\pm1} - c_l}{\Delta x_l}\right], \tag{20}$$

$$\left[\frac{\partial T}{\partial x}\right]_{l\pm\frac{1}{2}} = \pm\left[\frac{T_{l\pm1} - T_l}{\Delta x_l}\right]. \tag{21}$$

3.1. Koren HR-FVS

According to the first order method, the values of concentration and with temperature of the cell-interface in Eqs. (16)

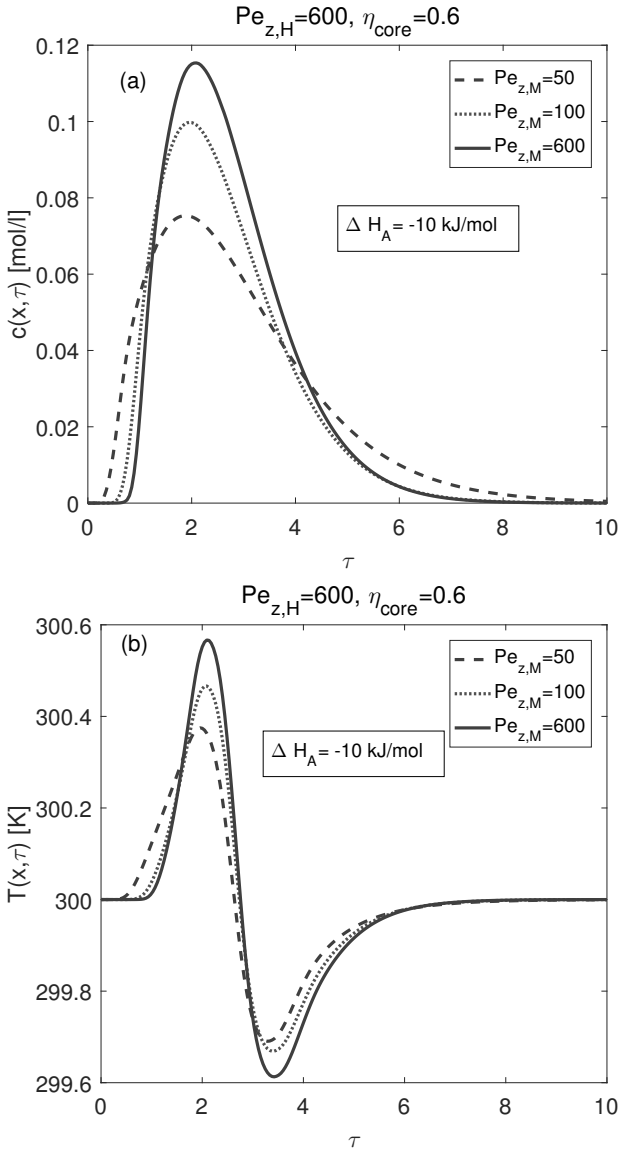

Figure 3: Influence of $\mathrm{Pe}_{z,M}$ on the model of non isothermal for the single-component elution by utilising two different η_{core} values. Table 1 lists all of the other parameter values that were considered

and (17) are approximated as numerically

$$c_{l+\frac{1}{2}} = c_l, \quad c_{l-\frac{1}{2}} = c_{l-1},$$
$$T_{l+\frac{1}{2}} = T_l, \quad T_{l-\frac{1}{2}} = T_{l-1}. \tag{22}$$

For the second-order HR-FVS, the developing flux-limiting formula is utilized in Eqs. (16) and (17) to numerically approximate the values of temperature and concentration of the cell interface [9, 30]:

$$c_{l+\frac{1}{2}} = c_l + \frac{1}{2}\Phi_1(\Gamma_{l+\frac{1}{2}})(c_l - c_{l-1}), \tag{23}$$

$$T_{l+\frac{1}{2}} = T_l + \frac{1}{2}\Phi_2(\Lambda_{l+\frac{1}{2}})(T_l - T_{l-1}), \tag{24}$$

Here, the symbols Φ_1 and Φ_2 are the flux-limiting formula for the concentrations and temperature, respectively. Also, $\Gamma_{l+\frac{1}{2},j}$ and $\Lambda_{l+\frac{1}{2},j}$ are the concentration and temperature gradient ratios, accordingly.

$$\Gamma_{l+\frac{1}{2},j} = \frac{c_{l+1} - c_l + \delta}{c_l - c_{l-1} + \delta}, \quad \Lambda_{l+\frac{1}{2}} = \frac{T_{l+1} - T_l + \delta}{T_l - T_{l-1} + \delta}. \tag{25}$$

In order to avoid division by zero, we have taken the value of $\delta = 10^{-10}$. Moreover, the limiting functions are expressed as

$$\Phi_1(\Gamma_{l+\frac{1}{2},j}) = \max\left[0, \min\left(2\Gamma_{l+\frac{1}{2},j}, \min\left(\frac{1}{3} + \frac{2}{3}\Gamma_{l+\frac{1}{2},j}\right)\right)\right], \tag{26}$$

$$\Phi_2(\Lambda_{l+\frac{1}{2},j}) = \max\left[0, \min\left(2\Lambda_{l+\frac{1}{2},j}, \min\left(\frac{1}{3} + \frac{2}{3}\Lambda_{l+\frac{1}{2},j}\right)\right)\right], \tag{27}$$

where $\Phi_1(\Gamma_{l+\frac{1}{2},j})$ and $\Phi_2(\Lambda_{l+\frac{1}{2},j})$ are sequentially defined for the concentration and temperature. Likewise, $c_{l-\frac{1}{2}}$ and $T_{l-\frac{1}{2}}$ can be evaluated by just replacing the index l by $l-1$ in the equations above. Finally, the built-in Rk-45 in Matlab is used to simulate the resulting ODE-system in Eqs. (16) and (17). The entire scheme described above was programmed and simulated in MATLAB.

4. Evaluating criterion for the process performance

In this section, we presents an evaluation for the performance criterion that can be utilized to improve product quality, according to the findings of Hováth and Fellinger [29] research. For applications to industries, preparative chromatographic methods required to be optimized in terms of their yield, productivity and efficiency. To describe this criterion procedure, we used a two-component mixture with component 2 having a higher reference affinity to the solid phase than component 1. i.e. $a^1_{\mathrm{ref}} < a^2_{\mathrm{ref}}$. Let ζ^1 represent the non-dimensional time when the fraction of component 1 be more than an appropriate benchmark (i.e, $c_1 < \epsilon c_{1,\mathrm{inj}}$), where $\epsilon = 10^{-6}$. In a similar way, let ζ^2 stand for a non-dimensional time when the concentration of component 2 drops below a particular level ($c_2 < \epsilon c_{2,\mathrm{inj}}$). The amount of time that has elapsed between the injections of consecutive two values, i.e. as cycle time, is represented by ζ^{cyc} and is written as

$$\zeta^{\mathrm{cyc}} = \zeta^2 - \zeta^1. \tag{28}$$

The cut time is defined as the time it takes to complete component 1 fractionation

$$\mathrm{Pur} = \frac{\int_{\zeta^1}^{\zeta^{\mathrm{cut}}} c_1(x=1,\zeta)d\zeta}{\int_{\zeta^1}^{\zeta^{\mathrm{cut}}} [c_1(x=1,\zeta)d\zeta + c_2(x=1,\zeta)d\zeta]}, \tag{29}$$

where

$$c_k(x=1,\zeta) = 2\int_0^1 c_k(x=1,\eta,\zeta)\eta d\eta, \quad k = 1,2. \tag{30}$$

The productivity (Pr) is defined by the quantity of a required compound manufactured per cycle's time. Also, the purity of

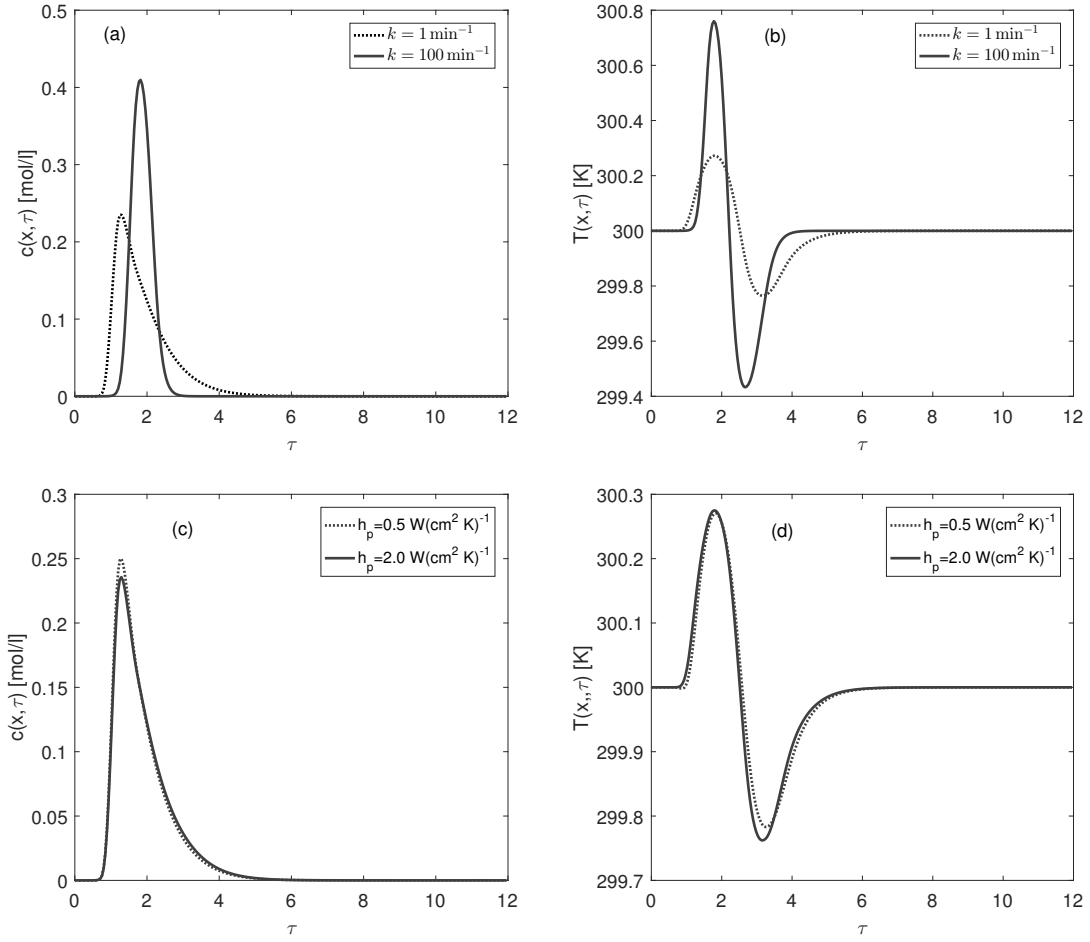

Figure 4: Impacts of both coefficients of mass as well as transfer of heat (k and h_p) for unchanged $\eta_{core} = 0.8$ and $\Delta H_A = -10\,\mathrm{kJ/mol}$. Table 1 lists all of the other parameter values that were considered

the suitable peak area is placed equal to 99%. For component 1, it is obtained as

$$\mathrm{Pr} = \frac{\int_{\zeta^1}^{\zeta^{cut}} c_1(x=1,\zeta)d\zeta}{\zeta^{cyc}}. \tag{31}$$

The proportion of considered component evaluated in segregated order and the complete amount of that injected component over the column inlet is referred as the quantity yield (Y). For the component 1 case, it is obtained as

$$\mathrm{Y} = \frac{\int_{\zeta^1}^{\zeta^{cut}} c_1(x=1,\zeta)d\zeta}{\int_{\zeta^1}^{\zeta^2} c_1(x=1,\zeta)d\zeta}. \tag{32}$$

5. Numerical test cases

Numerous numerical test cases for simulating the influences of η_{core}, $\mathrm{Pe}_{z,M}$, k and h_p, on the elution profiles are presented in this section. These characterize the core radius fraction, the axial Peclet number, the mass transfer coefficient and the heat transfer coefficient, respectively. In addition, we have taken the nonlinearity coefficients zero (i.e., $b_\iota = 0$ l/mol in Eq. (5)). Moreover, a process performance criterion for the parameters ζ^{cyc}, ζ^{cut}, Pr, and Y are simulated. Furthermore, the solute is injected through the column inner zone in all of the cases we investigated. In the plots in Figures 2-7, the solute component is denoted as c. While, the mobile phase temperature is denoted by the symbol T. The values of all needed parameters are taken from the scopes used in the applications of HPLC [32] and are classified in Table 1.

In Figure 2, we display the elution profile plots of both concentration and temperature of a single-component solute, for three distinct values of η_{core} (i.e. $\eta_{core} = 0, 0.4, 0.8$). Additionally, the value of adsorption enthalpy of the process is taken as $\Delta H_A = -10\,\mathrm{kJ/mol}$. It is obvious that operation of non-isothermal results in notable temperature differences within the column, as shown in given Figure 2(b). As shown in Figure 2(a), these temperature variations have no visible effect on the concentration profile due to the considered low value of ΔH_A. It is also worth noting that as η_{core} increases from 0 to 0.8 increases, the elution profiles become sharper, and as a result, their retention times reduce accordingly, i.e. By increasing the value of η_{core}, the column efficiency gradually improves. At

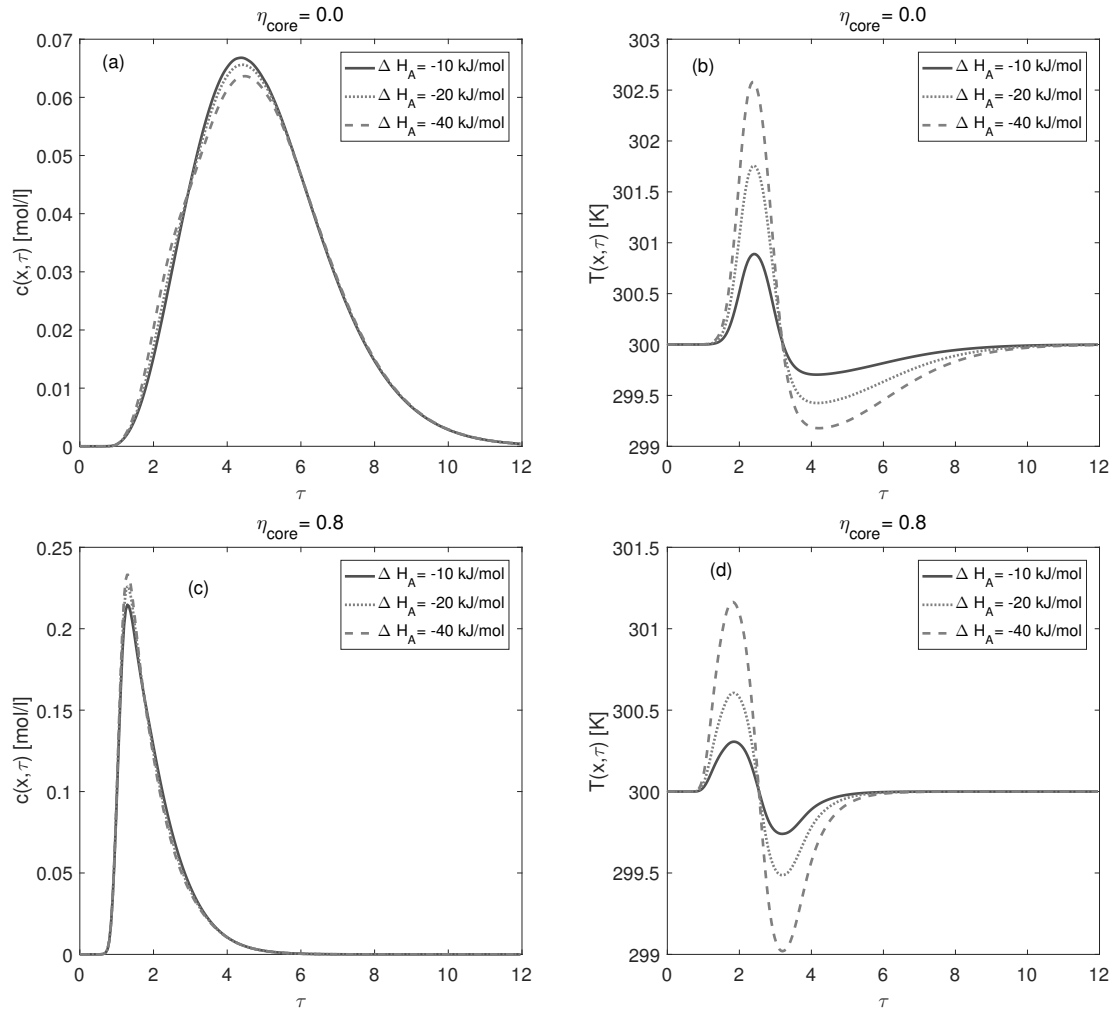

Figure 5: Effects of ΔH_A on the model of non-isothermal for single-component elution including two different values of ξ_{core}. Specifically, plots in 2-D for the single solute elutions profiles are presented at $\xi_{core} = 0$ & $\xi_{core} = 0.8$. Table 1 lists all of the other parameter values that were employed

the same time, the column's absorption capacity gradually decreases due to a reduce in the thickness of the layer including in porous.

Figure 3 demonstrates the impact of the non-dimension parameter $\mathrm{Pe}_{z,M}$ of concentration and temperature on the profiles of elution by utilizing the value of $\eta_{core} = 0.6$ and an unchanged value of $\mathrm{Pe}_{z,M} = 600$. The lesser value of $\mathrm{Pe}_{z,M}$ develops wider (spread) peaks, and thus the column efficiency decreases. In contrast, a higher $\mathrm{Pe}_{z,M}$ value results in narrower peaks, which improves column performance. All plots clearly show analogous impacts of different $\mathrm{Pe}_{z,M}$.

Figure 4 illustrates the results of k and h_p for an unchanged $\eta_{core} = 0.8$. It is clear that lower values of these dimension parameters result in broader elution profiles, while for high values of these parameters, the profiles are sharpened. The plots also show that the parameter h_p has a minor influence on the given profiles, whereas k has a significant impact on both profiles.

Figure 5 presents the influence of ΔH_A on the eluent profile for two distinct η_{core} values of a single-solute. As the operating condition for non-isothermal ($\Delta H_A = -10, -20$ & -40 kJ/mol) produces remarkable temperature differences, as it's clearly observed from Figure 5. Also, increasing the magnitude of ΔH_A affects the solute profile as well, and causing the concentration profile to become sharper while the peak moves upward. Further, variation of the particles size of core-shell decreases the retention time of the solute profile by making them narrower and sharper.

In Figure 6, for isothermal and non-isothermal conditions, we describe a process performance by simulating the following terms: ζ^{cyc}, ζ^{cut}, Pr, and Y (c.f. Eq. (28)-(29)) over η_{core} for $\Delta H_A = -10$ kJ/mol. It can be clearly observed that the time cycle as well as the cut time is decreasing from 36 to 12 and 97 to 10, respectively, as varies from entirely particles that are porous i.e. η_{core}=0.0 to the particles of core shell i.e. η_{core}=0.8. Moreover, a rise in the productivity can be seen up to $\eta_{core} = 0.74$ and it gradually falls later. Furthermore, the Y continuously increases for an upward increment of the η_{core} value. So, the cycle time, cut time, productivity and yield profiles are similar

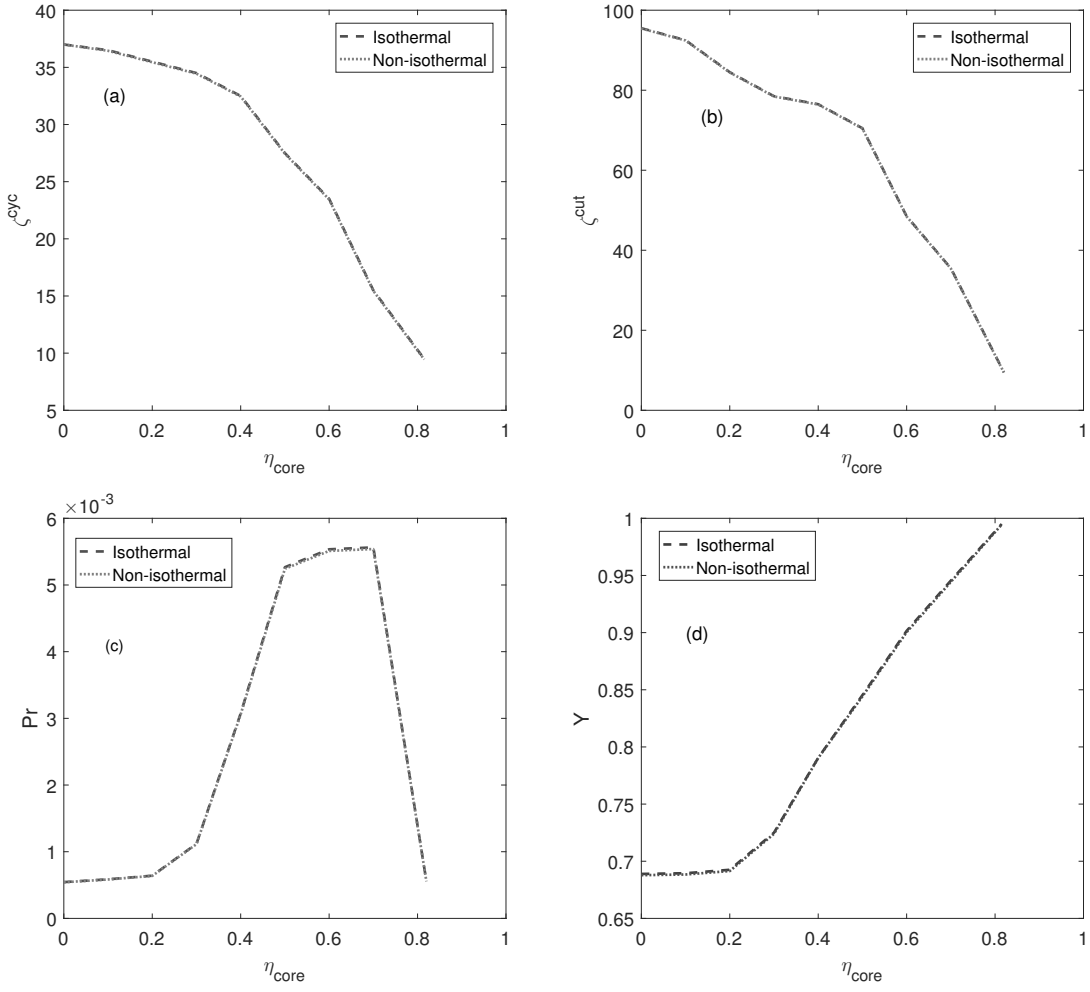

Figure 6: Isothermal and non-isothermal comparison for the process performance assessment. Here, the value for $\Delta H_A = -40\,\text{kJ/mol}$ is taken for the model of non isothermal process operating condition. Firstly, the plot (a) presents ζ^{cyc}, secondly, the plot (b) shows ζ^{cut}, thirdly the plot (c) depicts productivity (Pr) and the last plot (d) displays yield (Y) represents as a functions of η_{core} for $c_{1,\text{inj}} = 1 = c_{2,\text{inj}}$. Table 1 lists all of the other parameter values that were considered

for both isothermal and non-isothermal operations, as presented in Figure 5.

In Figure 7, we discussed a performance process to the assessment for both conditions of isothermal and non-isothermal. However, here we change the magnitude of ΔH_A from $\Delta H_A = -10\,\text{kJ/mol}$ to $\Delta H_A = -40\,\text{kJ/mol}$ over η_{core}. The cycle and cut times are both decreasing, as can be seen from varying 36 to 12 and 97 to 10, respectively, when we get away from particles that are completely porous (i.e. η_{core}=0.0) to the particles of core-shell (i.e. η_{core}=0.8). Similarly, the performance ascends upward and drops thereafter around $\eta_{core} = 0.74$. Moreover, the yield rises upward continuously. However, significant deviations in the cycle time and productivity profiles of non-isothermal and isothermal operations are detected. In the case of non-isothermal operating conditions, the reduction in cycle time decelerates slightly, but yield and productivity improve.

6. Conclusion

The effects of temperature variations were theoretically investigated on fixed-bed columns filled with core-shell particles. For that purpose, a nonlinear 1D-LKM was developed and solved numerically. It was found that rapid and better separations of complex samples can be obtained in columns filled with core-shell particles. The findings showed that profiles with sharper peaks and shorter residence times are produced by core radius fractions with higher values. Thus, the diffusion path within the adsorbents was reduced, which boosted the column's efficiency. Furthermore, the numerical results show that heat and concentration front interactions were investigated, which indicates an increase in the process performance assessment. Consequently, HPLC can be optimized by using core-shell particles with a sufficient core radius fraction loaded in the column.

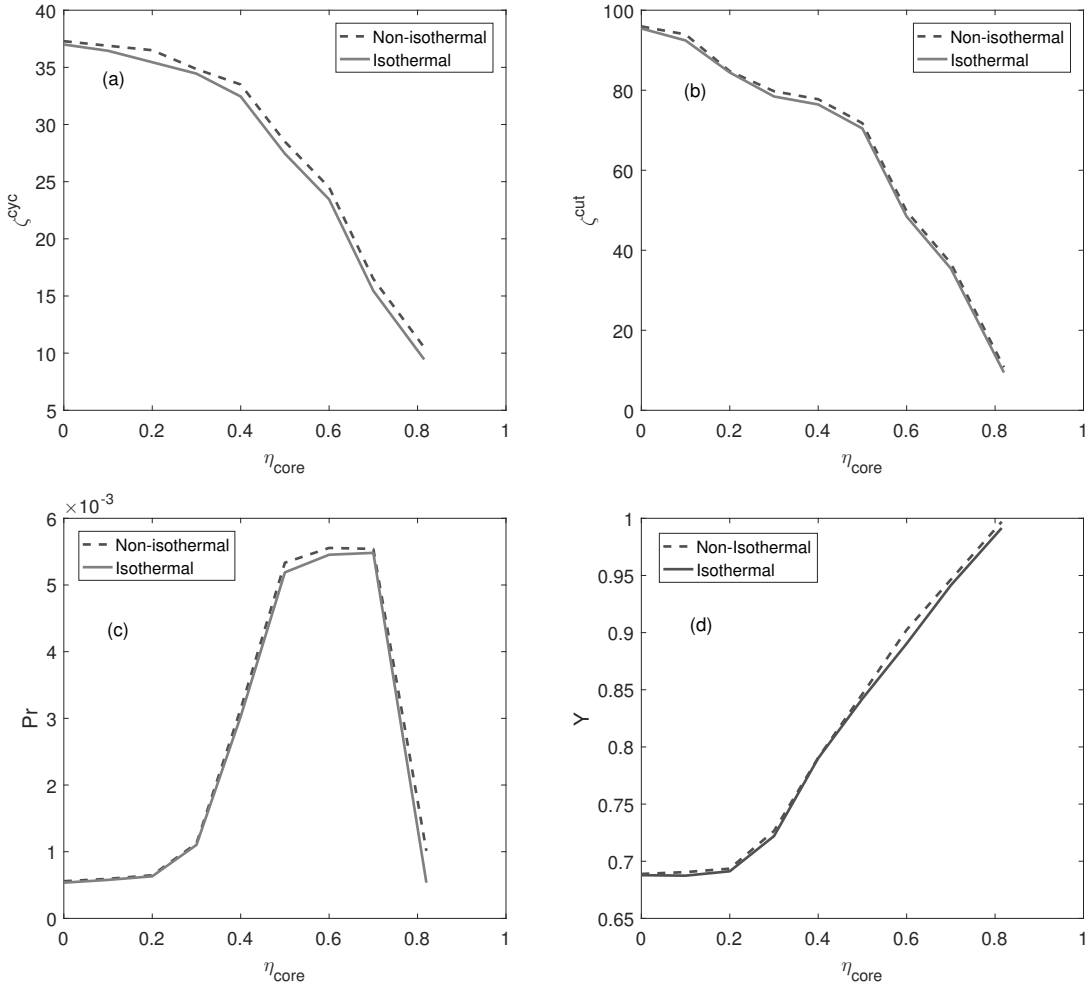

Figure 7: Isothermal and non-isothermal process comparison for the process performance assessment. Specifically, the value for $\Delta H_A = -40\,\text{kJ/mol}$ is taken for the process of non-isothermal operating condition. In the first plot (a) presents ζ^{cyc}, moving to second plot (b) shows ζ^{cut}, as well as the third plot (c) depicts productivity (Pr) and the last plot (d) displays yield (Y) represents as functions of η_{core} for $c_{1,\text{inj}} = 1 = c_{2,\text{inj}}$. Table 1 lists all of the other parameter values that were considered

Acknowledgements

The authors would like to express their sincere thanks for the financial support given by the National Mathematical Centre Abuja, Nigeria.

References

[1] G. Guiochon, A. Felinger, D. G. Shirazi & A. M. Katti, *Fundamentals of Preparative and Nonlinear Chromatography*, Elsevier Academic Press, New York (2006).

[2] D. M. Ruthven, *Principles of Adsorption and Adsorption Processes*, Wiley-Interscience, New York (1984).

[3] G. Guiochon, "Preparative Liquid Chromatography", Journal of Chromatography A **965** (2002) 129.

[4] T. Gu, M. Liu, K. S. C. Cheng, S. Ramaswamy, & C. A. Wang, "General rate model approach for the optimization of the core radius fraction for multicomponent isocratic elution in preparative nonlinear liquid chromatography using cored beads", Chemical Engineering Science 66 (2011) 3531.

[5] J. J. Kirkland, F. A. Truszkowski, C. H. Dilks & G. S. Engel, "Superficially porous silica microspheres for fast high-performance liquid chromatography of macromolecules", Journal of Chromatography A **890** (2000) 3.

[6] Y. Q. Xiang, B. W. Yan, C. V. McNeff, P. W. Carr & M. L. Lee, "Synthesis of micron diameter polybutadiene-encapsulatednon-porous zirconia particles forultra-high pressure liquid chromatography", Journal of Chromatography A **983** (2003) 83.

[7] J. Ning, F. Z. Kong, D. H. Li & Y. Z. Du, "Preparation of monodisperse agglomerated pellicular anion-exchange resins compatible with high-performance liquid chromatography solvents for ion chromatography", Journal of Chromatography A **793** (1998) 193.

[8] K. Kaczmarski & G. Guiochon, "Modeling of the mass-transfer kinetics in chromatographic columns packed with shell and pellicular particles", Analytical Chemistry **79** (2007) 4648.

[9] U. D. Uche, M. Uche, & F. Okafor, "Numerical solution of a two-dimensional model for non-isothermal chromatographic reactor packed with core-shell particles", Journal of the Nigerian Mathematical Society **3** (2021) 97.

[10] U. D. Uche, M. Uche, F. Okafor & K. Utalor, "Modeling and simulation of isothermal reactive liquid chromatography for two component elution-effects of core-shell particles", International Journal of Mathematical Sciences and Optimization: Theory and Applications **8** (2022) 117.

[11] U. D. Uche & M. Uche, "Theoretical Analysis of Linearized Non-isothermal Two-dimensional Model of Liquid Chromatography Columns Packed with Core-Shell Particles", International Journal of Applied and Computational Mathematics **7** (2021) 83.

[12] A. Brandt, G. Mann & W. Arlt, "Temperature Gradients in Preparative High-performance Liquid Chromatography Columns", Journal of Chromatography A **768** (1997) 109.

[13] T. Sainio, M. Kaspereit, A. Kienle & A. Seidel-Morgenstern, "Thermal Effects in Reactive Liquid Chromatography", Chemical Engineering Science **62** (2007) 5674.

[14] H. Poppe, J. C. Kraak, J. F. K. Huber & J. H. M. Van den Berg, "Temperature Gradients in HPLC Columns Due to Viscous Heat Dissipation", Chromatographia **14** (1981) 515.

[15] A. G. Ahmad & S. Qamar, "Effect of temperature variations on non-equilibrium and non-isothermal two-component liquid chromatography in cylindrical columns", Journal of Liquid Chromatography and Related Technology **43** (2020) 890.

[16] A. G. Ahmad, S. Qamar & A. Seidel-Morgenstern, "Linearized non-equilibrium and non-isothermal two-dimensional model of liquid chromatography for studying thermal effects in cylindrical columns", Journal of Liquid Chromatography and Related Technology **42** (2019) 436.

[17] H. W. Haynes Jr, "An Analysis of Sorption Heat Effects in the Pulse Gas Chromatography Diffusion Experiment", AIChE Journal **32** (1986) 1750.

[18] Y. Guillaume & C. Guinchard, "Prediction of Retention Times, Column Efficiency, and Resolution in Isothermal and Temperature-programmed Gas Chromatography: Application for Separation of Four Psoalens", Journal of chromatography Science **35** (1997) 14.

[19] G. Peter, Robinson & L. O. Allan, "Comparison of Isothermal and Non-linear Temperature Programmed Gas Chromatography the Temperature Dependence of the Retention Indices of a Number of Hydrocarbons on Squalane and SE-30", Journal of Chromatography A **57** (1971) 11.

[20] F. Gritti, M. Michel Martin & G. Guiochon, "Influence of Viscous Friction Heating on the Efficiency of Columns Operated Under Very High Pressures", Analytical Chemistry **81** (2009) 3365.

[21] T. Teutenberg, *High-temperature Liquid Chromatography: A Users Guide for Method Development*, RSC Chromatography Monographs (2010).

[22] F. D. Antia & C. Horvath, "High-performance Liquid Chromatography at Elevated Temperatures: Examination of Conditions for the Rapid Separation of Large Molecules", Journal of Chromatography A **435** (1988) 1.

[23] D. C. Snyder & J. W. Dolan, "Initial Experiments in High-performance Liquid Chromatographic Method Development I. Use of a Starting Gradient Run", Journal of Chromatography A **721** (1996) 3.

[24] L. R. Snyder, J. W. Dolan & D. C. Lommen, "Drylab® Computer Simulation for High-performance Liquid Chromatographic Method Development: I. Isocratic Elution", Journal Chromatography A **485** (1989) 45.

[25] A. I. Anya, U. Ofe & A. Khan, "Mathematical Modeling of Waves in a Porous Micropolar Fibrereinforced Structure and Liquid Interface", Journal of the Nigerian Society of Physical Sciences **4** (2022) 823.

[26] F. O. Akinpelu, R. A. Oderinu & A. D. Ohagbue, "Analysis of hydromagnetic double exothermic chemical reactive flow with connective cooling through a porous medium under bimolecular kinetics", Journal of the Nigerian Society of Physical Sciences **4** (2022) 130.

[27] M. Suzuki & J. M. Smith, "Kinetic Studies by Chromatography", Chemical Engineering Science **26** (1971) 221.

[28] S. Qamar, N. Kiran, T. Anwar, S. Bibi & A. Seidel-Morgenstern, "Theoretical Investigation of Thermal Effects in an Adiabatic Chromatographic Column Using a Lumped Kinetic Model Incorporating Heat Transfer Resistances", Indusrial & Engineering Chemical Research **57** (2015) 2287.

[29] K. Horváth & A. Felinger, "Influence of particle size and shell thickness of core-shell packing materials on optimum experimental conditions in preparative chromatography", Journal of Chromatography A **407** (2015) 100.

[30] S. Qamar, S, Perveen & A. Seidel-Morgenstern, "Numerical Approximation of Nonlinear and Non-equilibrium Two-dimensional Model of Chromatography", Computers & Chemical Engineering **94** (2016) 411.

[31] P. V. Danckwerts, "Continuous flow systems", Chemical Engineering Science **2** (1953) 1.

[32] T. D. Vu & A. Seidel-Morgenstern, "Quantifying temperature and flow rate effects on the performance of a fixed-bed chromatographic reactor", Journal of Chromatography A **1218** (2011) 8097.